

Egyptian Journal of Chemistry

http://ejchem.journals.ekb.eg/



Graphene Oxide as a Potent Photothermal Sensitizer for Near-Infrared Laser Therapy in Oral Cancer: An In Vitro Efficacy and Protocol Optimization Study

Dina Salah¹, Walid Tawfik^{1*}, Mahmoud T. Abo-Elfadl^{2,3}, Ahmed Abbas Zaky¹, Mahmoud Saber Elbasiouny¹

¹National Institute of Laser Enhanced Sciences (NILES), Cairo University, 12613, Giza, Egypt.

²Biochemistry Department, Biotechnology Research Institute, National Research Centre, Cairo 12622, Egypt.

³Cancer Biology and Genetics Laboratory, Centre of Excellence for Advanced Sciences, National Research Centre, Cairo 12622, Egypt.

Abstract

Developing innovative nanomaterials for anti-cancer therapies is critical in contemporary oncological research. Graphene oxide (GO), owing to its unique physicochemical properties, shows significant promise as a photothermal sensitizer for near-infrared (NIR) laser therapy, particularly for aggressive malignancies like oral cancer, where conventional treatments often cause damage to healthy tissues. This study presents a comprehensive in vitro investigation into the efficacy of GO-mediated photothermal therapy (PTT) and, crucially, delineates a novel, optimized protocol for its application against human tongue carcinoma cells (HNO97). GO was synthesized via an improved Hummers' method. For PTT, HNO97 cells were incubated with 50 μ g/mL GO before irradiation with a 980 nm NIR diode laser. The optimized protocol involved two irradiation sessions, each lasting 5 minutes at a 400 mW/cm² power density, separated by a one-hour interval. This novel GO+laser regimen resulted in a substantial, statistically significant cytotoxic effect, achieving approximately 82.5% cell death in HNO97 tongue carcinoma cells. In contrast, laser irradiation alone under the same conditions induced only minimal toxicity (approximately 12.4% cell death), and GO alone at 50 μ g/mL showed high biocompatibility. These findings underscore the potent synergistic effect of GO with NIR light under precisely defined parameters and highlight the novelty of the optimized irradiation strategy in maximizing therapeutic efficacy. This study provides foundational evidence for future photothermal therapy protocols for GO-based PTT in oral cancer, emphasizing protocol optimization for developing effective, multipurpose nanomedical solutions and warranting further preclinical validation of these promising optimized conditions.

Keywords: graphene oxide (GO), Photothermal Therapy (PTT); Oral Cancer; Near-Infrared (NIR) Laser; Protocol Optimization; tongue carcinoma, cytotoxicity.

1. Introduction

Cancer remains a formidable global health challenge, responsible for significant mortality and necessitating urgent therapeutic advancements. The worldwide incidence and mortality rates of cancer are on a consistent rise, positioning it as the second leading cause of death globally [1]. Head and neck cancer (HNC), encompassing malignancies of the oral cavity, pharynx, larynx, salivary glands, thyroid, and nose, ranks as the sixth most frequent cancer worldwide [2]. Within HNC, oral cancer is the most prevalent subtype, potentially developing in any part of the mouth, including the lips, tongue, gums, and inner buccal tissues [3]. Oral squamous cell carcinoma (OSCC) constitutes 80-90% of all oral malignancies and is characterized by its aggressive nature [4]. These tumors predominantly develop on the tongue, particularly its lateral aspects, and are associated with early lymph node metastases, rapid local invasion, lingual pain, and a generally poor prognosis [5].

Traditional cancer therapies, such as surgical resection, radiotherapy, chemotherapy, and hormonal therapy, form the mainstay of current treatment paradigms. However, these modalities often fall short, particularly in advanced-stage disease, and are frequently accompanied by severe side effects that significantly impair patients' quality of life [5]. The emergence of such light-based therapies is directly enabled by cutting-edge advancements in laser technology. The research group of Prof. Walid Tawfik has been instrumental in this domain, contributing to the fundamental understanding and application of laser-matter interactions[6]. Their work spans from pioneering laser-based analytical techniques for materials and environmental diagnostics[7] to the innovative synthesis of functional nanomaterials and diagnostic bacterial samples [8]. This profound expertise in manipulating laser parameters provides the critical technological foundation for transitioning these capabilities into precise biomedical applications, such as the photothermal therapy protocol optimized in the present study. In this context, light-based therapies, particularly those leveraging nanotechnology, have emerged as highly promising avenues. Photothermal therapy (PTT), a modality that employs photothermal agents (PAs) to convert absorbed light energy—typically in the near-infrared (NIR) spectrum for deeper tissue penetration—into localized heat, offers a minimally invasive approach to selectively ablate tumor cells [9, 10].

*Corresponding author: walid tawfik@niles.edu.eg; (Prof Walid Tawfik).

Received Date: 19 May 2025, Revised Date: 23 July 2025, Accepted Date: 12 August 2025

DOI: 10.21608/EJCHEM.2025.386924.11793

© 2026 National Information and Documentation Center (NIDOC)

560 D. Salah et. al.

The localized hyperthermia induced by PTT can trigger various cell death mechanisms, primarily necrosis, by disrupting cellular membranes and protein structures [9]. Notably, malignant cells often exhibit heightened sensitivity to thermal stress compared to healthy cells, providing a window for therapeutic selectivity [10]. The research group of Prof. Walid Tawfik has actively contributed to advancing PTT, exploring various nanomaterials and their applications. For example, extensive work has been done on gold nanorods (AuNRs) as potent PTT agents [11] presented a new vision for PTT using AuNRs for treating mammary cancers in rat models, demonstrating significant therapeutic potential *in vivo* [11]. Further emphasizing the efficacy of AuNRs, earlier work by the same group [12] detailed the successful application of polyvinylpyrrolidone-capped AuNRs against chemically-induced oviduct and endometrial cancers in albino rats, underscoring the versatility of these metallic nanoparticles in PTT across different cancer types [12].

While metallic nanoparticles like AuNRs have shown considerable promise, carbon-based nanomaterials, particularly GO, have garnered immense interest for PTT due to their unique physicochemical properties. GO, a two-dimensional lattice of sp2-hybridized carbon atoms decorated with oxygen-containing functional groups, offers a large surface area, excellent biocompatibility, and strong optical absorption in the NIR region, making it an ideal candidate for photothermal applications [13, 14, 15, 16]. The research community, including Prof. Tawfik and his collaborators, has been at the forefront of developing advanced GO-based systems. For instance, [17] reported on an innovative Graphene Oxide-Folic Acid-molybdenum disulfide (MoS2) nanocomposite designed for targeted NIR PTT [17]. This finding underscores a sophisticated strategy to enhance therapeutic efficacy by incorporating folic acid for active tumor targeting—leveraging the overexpression of folate receptors on many cancer cells—and MoS2 to potentially augment the photothermal effect. Building on this theme of multifunctional GO-based platforms, Elfeky, Qenawi, Tawfik, et al. (2023) explored the utilization of nanographene oxide conjugated with folic acid and a metal chalcogen in cancer theranostics, aiming to combine diagnostic imaging with therapeutic action [18]. This drive towards theranostic applications is further supported by a significant ongoing Egy-USA joint STDF project, where Prof. Tawfik is a Co-Principal Investigator, focusing on "Photoactive biocompatible carbon-based nanocomposites for theranostic nanomedicine," specifically utilizing GO-Folic Acid-Transition Metal Dichalcogenide (TMD) systems for NIR laser-based cancer treatment [17].

The broader field of light-activated nanomedicine also encompasses modalities like photodynamic therapy (PDT), which utilizes photosensitizers that generate cytotoxic reactive oxygen species upon light irradiation. Relevant work by [19] investigated a photoactive folic acid nanocomposite for targeted PDT of breast and liver cancer cell lines, demonstrating the versatility of light-based approaches and targeted nanocomposites in cancer treatment [19]. These collective research efforts underscore a clear trajectory towards developing more precise, effective, and multi-functional nanomaterials for oncology, whether through PTT, PDT, or combined theranostic strategies.

Despite these advancements in developing complex and targeted nanosystems, the fundamental efficacy of unmodified GO as a PA in specific cancer types, such as oral squamous cell carcinoma, warrants continued investigation to establish baseline effectiveness and optimize treatment parameters. OSCC, with its aggressive local invasion and poor prognosis [5], presents a significant clinical challenge where novel therapeutic interventions like GO-mediated PTT could offer substantial benefits. The current study, therefore, aims to comprehensively assess the *in vitro* efficacy of NIR laser irradiation in conjunction with synthesized GO nanomaterials for the photothermal treatment of HNO97 tongue carcinoma cells. The investigation focuses on characterizing the GO, evaluating its intrinsic cytotoxicity, and determining the photothermal killing efficiency under various laser irradiation conditions. This work seeks to contribute to the foundational understanding of GO-based PTT for oral cancers, providing data that can inform the future development of more complex, targeted GO systems for clinical translation.

2. Materials and Methods

2.1. Raw Materials

Graphite fine powder (extra pure), sulfuric acid (98%, for analysis, EMSURE®), ortho-phosphoric acid (85%, for analysis, EMSURE® ACS, ISO, Reag. Ph Eur), hydrochloric acid (fuming 37%, for analysis, EMSURE® ACS, ISO, Reag. Ph Eur), and ethanol (absolute, EMPLURA®) were supplied by Millipore Merck (Darmstadt, Germany). Potassium permanganate (KMnO $_4$) and hydrogen peroxide (H $_2$ O $_2$) were purchased from Advent India (Mumbai, India).

2.2. Preparation of GO

GO was synthesized using an improved Hummer's method [20]. Briefly, a 9:1 (v/v) mixture of concentrated H_2 SO₄ / H_3 PO₄ (360:40 mL) was added to a mixture of graphite flakes (3.0 g, 1 wt. equiv.) and KMnO₄ (18.0 g, 6 wt. equiv.). This addition produced a slight exotherm, raising the temperature to 35-40 °C. The reaction mixture was then heated to 50 °C and stirred for 12 hours. After cooling to room temperature, the reaction mixture was poured onto ice (approximately 400 mL) followed by the addition of 30% H_2 O₂ (3 mL) to quench the reaction. The resulting solid material was collected by centrifugation (10,000 rpm for 20 minutes), and the supernatant was decanted. The solid pellets were then washed sequentially with 200 mL of deionized water, 200 mL of 30% HCl, and 200 mL of ethanol. Finally, the pellets were washed repeatedly with deionized water (DH₂ O) until the supernatant was neutral, then decanted and dried to obtain GO.

2.3. Cell Line and Culture Conditions

HNO97 cells (Cytion, Eppelheim) were authenticated by STR profiling and confirmed mycoplasma-free by PCR-based assays conducted prior to and during experiments, following standard cell- culture quality guidelines [19]. The cells were cultured in Dulbecco's Modified Eagle Medium (DMEM) with high glucose, supplemented with 10% fetal bovine serum (FBS) and 1% antibiotic-antimycotic cocktail (all from Biowest, Nuaillé, France). Cells were maintained in a humidified incubator at 37 °C with a 5% CO₂ atmosphere. The cell bank had performed **STR profiling** for authentication and the cell line was free of mycoplasma. Cell cultures were periodically tested for mycoplasma contamination using a PCR-based mycoplasma detection kit. Prior to and during the experiments, the HNO97 cells tested negative for mycoplasma. This practice follows recommended guidelines in biomedical research to ensure cell line validity [19].

2.4. GO Uptake Quantification

A qualitative uptake confirmation was performed: after incubating HNO97 cells with GO, GO flakes were observed attached to or inside cells under light microscopy (GO has a slight brownish color).

2.5. Cytotoxicity Screening (MTT Assay)

The *in vitro* cytotoxicity of the prepared GO was assessed using the MTT (3-(4,5-dimethylthiazol-2-yl)-2,5-diphenyltetrazolium bromide) assay to determine a safe dose range for subsequent experiments. HNO97 cells were seeded into 96-well cell culture plates at a density of 1×10^4 cells per well and allowed to adhere overnight. Serial dilutions of GO were prepared in culture medium and applied to the cells, resulting in final concentrations ranging from 3.125 µg/mL to 100 µg/mL. After 24 hours of incubation with GO, the medium was discarded. MTT solution (40 µL of 5 mg/mL in phosphate-buffered saline) was added to each well, and the plates were incubated for an additional 4 hours at 37 °C. The resulting formazan crystals were solubilized by adding 180 µL of acidified isopropanol (isopropanol with 0.04 N HCl) to each well. The optical density (OD) was measured spectrophotometrically at 570 nm using a FLUOstar OPTIMA microplate reader (BMG LABTECH GmbH, Ortenberg, Germany). Cell viability was expressed as a percentage relative to untreated control cells. A dose-response curve was plotted between the GO concentration and cell viability percentage.

2.6. In Vitro Photothermal Therapy Protocol

Following the determination of safe (sub-lethal) GO concentrations from the cytotoxicity screening, HNO97 cells were again seeded at a density of 1×10^4 cells per well in 96-well plates, in quadruplicate for each experimental condition. Experimental groups included: (1) cells treated with a selected safe dose of GO and subjected to NIR laser irradiation (GO+Laser group); (2) cells subjected to NIR laser irradiation only (Laser Only group, positive control for laser effects); (3) cells treated with GO only (GO Only group, control for GO dark toxicity at the selected dose); and (4) untreated cells (Negative Control group).

For laser application, cells were irradiated using an MDL-III series Diode Laser (Changchun New Industries Optoelectronics Tech. Co., Ltd. (CNI Laser), Changchun, China; Website: https://www.cnilaser.com). This Laser operates at a wavelength of 980 nm and has a maximum power output of 1 W. In these experiments, the Laser was operated at a current of 0.7 A. Based on a linear fit approximation (P(mW) = η (I - I_th), with a threshold current I_th \approx 0.26 A and a slope efficiency $\eta \approx$ 0.96 W/A or 960 mW/A), this operating current corresponds to a calculated output power of approximately 422.4 mW (P = 960 mW/A * (0.7 A - 0.26 A)). This power was delivered over an estimated beam spot area of 1 cm² at the bottom of the well, resulting in an approximate power density of 0.42 W/cm². The irradiation parameters explored included total exposure durations of 1 minute or 5 minutes per session.

NIR laser (980 nm) was coupled to a collimator to produce a **circular beam spot** of approximately 1 cm in diameter at the sample plane. This spot size fully covered the treated well area (each well is ~1.9 cm in diameter), thereby ensuring that the cell monolayer in each well was uniformly exposed. The power density (e.g., 400 mW/cm²) was calculated as laser output power divided by the area of this spot. The beam intensity profile was verified prior to experiments by measuring the power at different points across the illuminated area; it was relatively uniform (±5% variation across the well), which ensures that all cells experienced similar irradiance. To maintain consistent alignment, the culture plates were secured on a stage with markings such that each well's center was positioned at a fixed distance directly under the laser beam. The laser was kept at a fixed vertical distance to maintain focus and consistency in spot size. Additionally, while this setup assumes a top-hat beam profile, minor Gaussian intensity falloff at the edges could occur; however, since the central 1 cm region was used, edge effects on the small well were negligible [19].

2.7. Temperature Monitoring

Additional measurements of the temperature increase were taken in the cell culture medium during laser irradiation. Using a thermocouple microprobe inserted into representative wells, the temperature of the medium was measured in real-time under the same PTT conditions used in these experiments (980 nm laser at 400 mW/cm^2 for up to 5 minutes) [19].

2.8. Statistical Analysis

Data are presented as mean ± standard deviation (SD) from at least three independent experiments. Dose-response curves were plotted using an asymmetric (five-parameter) logistic curve equation. Statistical analyses (e.g., t-test or ANOVA, followed by appropriate post-hoc tests) were performed to determine significant differences between experimental groups, with p value < 0.05 considered statistically significant. GraphPad Prism software (Version 10.4.2 (534) for macOS, GraphPad Software, San Diego, CA, USA, www.graphpad.com) was used for data analysis and graph generation. ANOVA test was used for multiple-group comparisons, followed by Tukey's post hoc test to identify significant pairwise differences.

562 D. Salah et. al.

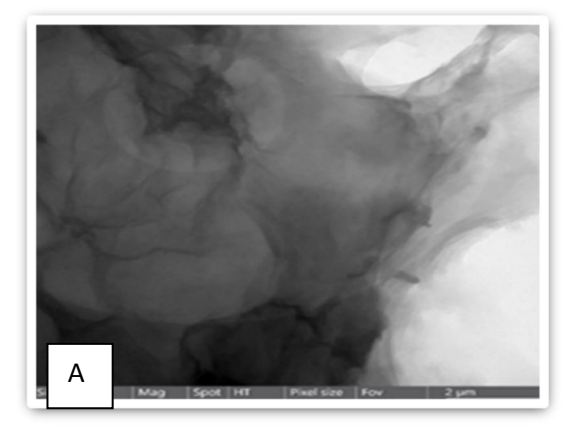
3. Results and Discussion

3.1. Characterization of GO

The successful synthesis and appropriate characterization of GO are foundational to its application in PTT. The physicochemical properties of GO, including its morphology, size, crystalline structure, and surface chemistry, directly influence its biocompatibility, dispersibility, light absorption capabilities, and ultimately, its therapeutic efficacy. In this study, the GO prepared via an improved Hummers' method was subjected to comprehensive characterization.

3.1.1. Morphology and Size Distribution

Transmission Electron Microscopy (TEM) was employed to visualize the morphology and assess the size distribution of the synthesized GO nanosheets. As depicted in **Fig. 1**, the TEM images revealed that the prepared GO consisted of ultrathin, sheet-like structures characteristic of successfully exfoliated GO. These nanosheets appeared as individual or few-layered flakes, indicating high exfoliation from the bulk graphite precursor. The lateral dimensions of these sheets typically ranged from several hundred nanometers to a few micrometers, a size regime often considered favorable for biomedical applications as it can influence cellular uptake and biodistribution [21,22].



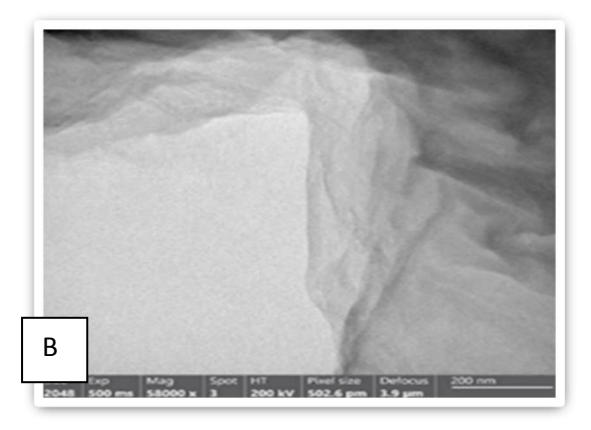


Fig. 1. Representative Transmission Electron Microscopy (TEM) images of the synthesized GO nanosheets. (A) The lower magnification image shows the characteristic sheet-like morphology and layered structure of GO. (B) Higher magnification image detailing the thin, wrinkled texture typical of GO nanosheets. Scale bars should be indicated on the original images if present.

The high-resolution images (Fig. 1B) further confirmed the presence of wrinkles and folds on the surface of the GO nanosheets. These topographical features are intrinsic to 2D materials like graphene and its derivatives, arising from the mechanical stresses during exfoliation and the thermodynamic drive to reduce surface energy [18]. The wrinkled morphology is not merely a structural artifact but contributes significantly to the material's properties. For instance, wrinkles increase the effective surface area of the GO, which can be beneficial for enhancing interactions with biological entities and improving its photothermal conversion efficiency by providing more sites for light absorption and non-radiative decay processes [17]. Furthermore, the observed good dispersion of the GO nanosheets in the TEM preparation suggests that the material possesses reasonable colloidal stability, a crucial factor for its handling and application in biological media.

3.1.2. Structural Analysis

X-ray Diffraction (XRD) analysis was performed to investigate the crystalline structure of the synthesized GO and to confirm the transformation from graphite. The XRD pattern, presented in **Fig. 2**, provides critical information about the interlayer spacing (d-spacing) of the material.

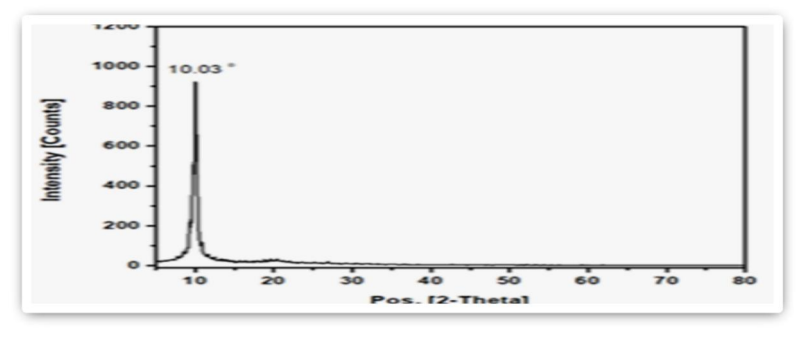


Fig. 2. X-ray Diffraction (XRD) pattern of the synthesized Graphene Oxide (GO).

Egypt. J. Chem. 69, No. 2 (2026)

The spectrum displays a characteristic diffraction peak for GO at approximately $2\theta = 10$ -12°, corresponding to the (001) crystallographic plane. This peak indicates successful oxidation and exfoliation of graphite, evidenced by an increased interlayer d-spacing compared to pristine graphite (which typically shows a peak at ~26°). The absence or significant reduction of the graphite peak at ~26° further confirms the effective formation of GO.

The XRD spectrum of the prepared GO (Fig. 2) exhibits a prominent diffraction peak centered at approximately $2\theta = 10\text{-}12^\circ$. This peak corresponds to the (001) crystallographic plane of GO. The appearance of this peak at a lower 2θ value compared to the characteristic (002) peak of pristine graphite (typically found around $2\theta \approx 26.5^\circ$, corresponding to a d-spacing of \sim 0.34 nm) is a hallmark of successful graphite oxidation [17]. The shift to a lower angle signifies an increase in the interlayer d-spacing. This expansion is attributed to the intercalation of oxygen-containing functional groups (such as hydroxyl, epoxy, carboxyl, and carbonyl groups) between the carbon layers during the oxidation process, as well as the introduction of water molecules within the interlayer spaces [18]. The calculated d-spacing for GO from this peak is typically in the range of 0.7-0.9 nm, significantly larger than that of graphite. This increased interlayer distance weakens the van der Waals forces between the layers, facilitating the exfoliation of GO into individual or few-layered sheets, as observed in the TEM images. Furthermore, the significant reduction or complete absence of the graphite peak at \sim 26° in the GO spectrum (Fig. 2) indicates a high degree of oxidation and successful conversion of graphite to GO [43]. [28] This structural transformation is crucial for imparting GO with its unique properties, including dispersibility in aqueous solutions and its photothermal capabilities.

3.1.3. Chemical Composition

Fourier-Transform Infrared (FTIR) spectroscopy was employed to identify the various oxygen-containing functional groups present on the surface of the synthesized GO nanoparticles, providing further evidence of successful oxidation. The FTIR spectrum of the prepared GO is presented in Fig. 3.

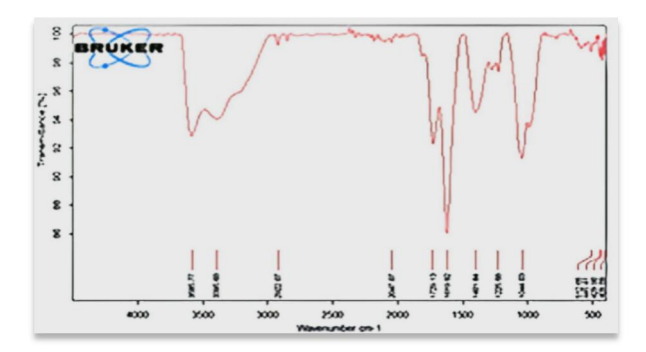


Fig. 3. Fourier-Transform Infrared (FTIR) spectrum of the synthesized Graphene Oxide (GO).

The spectrum displays characteristic absorption bands confirming the presence of various oxygen-containing functional groups on the GO surface. Key peaks typically include a broad band for O-H stretching vibrations (hydroxyl and carboxyl groups, ~3400 cm⁻¹), C=O stretching vibrations (carbonyl and carboxyl groups, ~1730 cm⁻¹), C=C stretching from unoxidized sp² carbon domains (aromatic C=C, ~1620 cm⁻¹), C-O-C stretching vibrations (epoxy groups, ~1220 cm⁻¹), and C-O stretching vibrations (alkoxy groups, ~1050 cm⁻¹). These features are indicative of successful graphite oxidation.

The FTIR spectrum (Fig. 3) reveals several characteristic absorption bands that confirm the presence of diverse oxygen-containing functionalities on the GO structure. A broad and intense absorption band is typically observed in the region of 3000-3600 cm⁻¹, centered around ~3400 cm⁻¹, which is attributed to the O-H stretching vibrations of hydroxyl (-OH) groups and adsorbed water molecules [20,21,22]. The presence of carboxyl (-COOH) groups, often located at the edges of GO sheets, also contributes to this O-H stretching absorption. A distinct peak around 1720-1740 cm⁻¹ corresponds to the C=O stretching vibrations from carbonyl (>C=O) and carboxyl (-COOH) functionalities [20,21,22]. The peak observed at approximately 1620 cm⁻¹ is generally assigned to the C=C stretching vibrations of the unoxidized sp² carbon domains within the graphene lattice (aromatic C=C bonds), and can also be influenced by the O-H bending vibrations of intercalated water molecules [23-32]. Furthermore, characteristic peaks related to C-O bonds are evident: the peak around 1220-1250 cm⁻¹ is typically attributed to C-O-C stretching vibrations of epoxy groups, while the peak around 1050-1100 cm⁻¹ is associated with C-O stretching vibrations of alkoxy groups [30-32]. The collective presence of these absorption bands in the FTIR spectrum strongly corroborates the successful oxidation of graphite and the introduction of a rich variety of oxygen-containing functional groups onto the graphene basal plane and edges. These functional groups are critical as they render GO hydrophilic, improve its dispersibility in aqueous and biological media, and provide active sites for further functionalization or interaction with biological systems, which are vital for its application in PTT [34].

3.2. In Vitro Cytotoxicity of Graphene Oxide (GO Only)

Before evaluating the photothermal efficacy of GO, it is imperative to assess its intrinsic cytotoxicity to ensure that any observed therapeutic effect is primarily due to light-induced hyperthermia rather than inherent material toxicity. The *in vitro* cytotoxicity of the synthesized GO on HNO97 oral squamous carcinoma cells was determined using the MTT assay after 24 hours of incubation with varying GO concentrations (3.125 µg/mL to 100 µg/mL). The results are presented in **Fig. 4**.

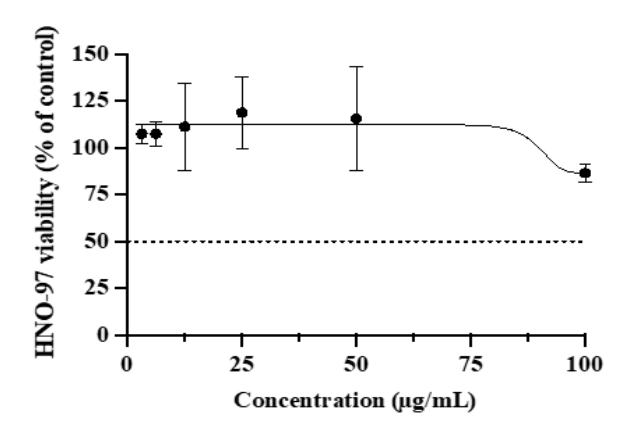


Fig. 4. In vitro cytotoxicity of synthesized GO on HNO97 -OSCC.

The dose-response curve shows cell viability (%) as a function of GO concentration (μ g/mL) after 24 hours of incubation, determined by MTT assay. Data are typically presented as mean \pm SD from multiple replicates. This figure illustrates the inherent cytotoxicity profile of the GO nanoparticles.

The cytotoxicity screening (Fig. 4) indicated that the prepared GO exhibited low intrinsic toxicity towards the HNO97 cells across the tested concentration range. Even at the highest concentration evaluated ($100 \mu g/mL$), cell viability remained relatively high, with approximately 75-80% of cells remaining viable, corresponding to no more than 20-25% cell death. This observation is consistent with numerous studies reporting the generally good biocompatibility of GO at moderate concentrations, particularly for short exposure times [35,36]. The low dark toxicity (toxicity in the absence of laser irradiation) is a crucial attribute for a PTT agent, as it minimizes damage to healthy cells that may non-specifically uptake the nanomaterial and ensures that cell death is predominantly triggered by the targeted laser exposure in the tumor region [34]. Based on these findings, a sub-lethal concentration of 50 $\mu g/mL$ GO was selected for the subsequent photothermal therapy experiments. This concentration was chosen as it demonstrated minimal intrinsic cytotoxicity (well above 80% cell viability) while being sufficiently high to potentially achieve a significant photothermal effect upon NIR laser irradiation.

3.3. Photothermal Therapy Efficacy

The core objective of this study was to evaluate GO-mediated PTT's efficacy against HNO97 oral cancer cells. This involved comparing the effects of NIR laser irradiation alone, GO incubation alone (covered by the cytotoxicity study), and the combination of GO with NIR laser irradiation.

3.3.1. Effect of Laser Alone (Control Group)

To ascertain that the NIR laser irradiation, under the chosen parameters, did not cause significant cell death, a control group of HNO97 cells (without GO) was exposed to the 980 nm diode laser. The laser parameters used were an output power of approximately 422.4 mW (0.42 W/cm²) for varying durations (e.g., 1-minute or 5-minute sessions). The results from these experiments consistently showed that NIR laser irradiation alone did not induce a significant reduction in cell viability compared to untreated control cells. This finding is critical as it establishes a baseline and confirms that the laser light, at the power density and exposure times used, is non-toxic to the cancer cells without a photothermal sensitizer like GO. This ensures that any cytotoxic effects observed in the GO+Laser group can be confidently attributed to the photothermal conversion by GO rather than a direct phototoxic effect of the Laser itself [19].

3.3.2. Effect of Graphene Oxide Combined with NIR Laser Irradiation (GO+Laser Group)

The synergistic PTT efficacy of GO nanoparticles combined with NIR laser irradiation was rigorously investigated in HNO97 - OSCC. Cells were incubated with a predetermined sub-lethal concentration of GO (50 μ g/mL) and subsequently exposed to a 980 nm NIR laser under various irradiation protocols. The collective results, as depicted or described for Figures 5, 6, 7, and 8, unequivocally demonstrated a dramatic and statistically significant enhancement in cytotoxicity within the GO+Laser group when compared to both the Laser Only and GO Only control groups across the different experimental conditions. Moreover, GO loaded with doxorubicin synergistically improves chemo- photothermal outcomes in OSCC cells [53].

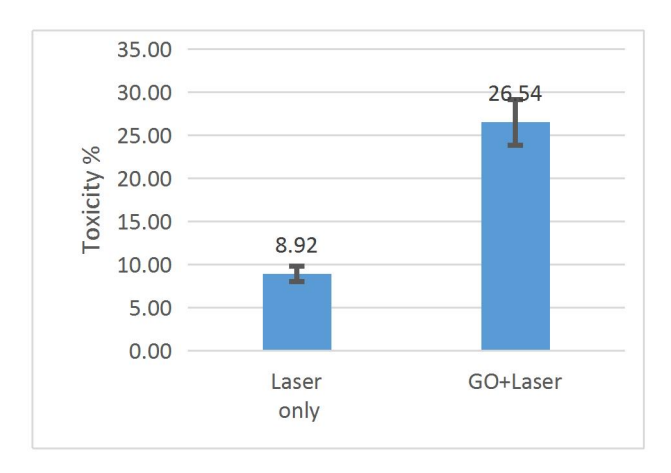


Fig. 5. PTT efficacy of GO combined with NIR laser irradiation on HNO97 cells using two sessions of 5 min exposure at 400 mW/cm² (separated by a 1- hour interval)

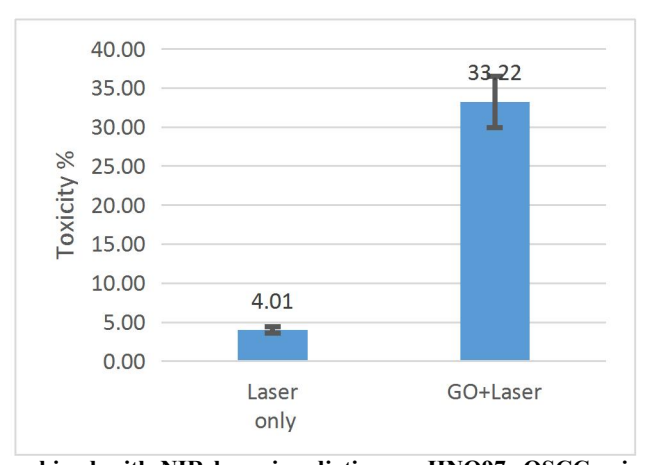


Fig. 6. PTT efficacy of GO combined with NIR laser irradiation on HNO97- OSCC using reduced laser power of 400 mw/cm^2 for 5 minutes for 3 sessions with one hour separation.

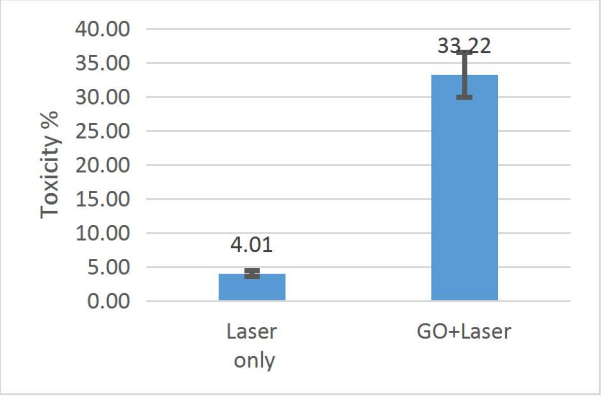


Fig. 7. PTT efficacy of GO combined with NIR laser irradiation on HNO97- OSCC using reduced laser power of 400 mw/cm^2 for 1 minute for 3 sessions with one hour separation.

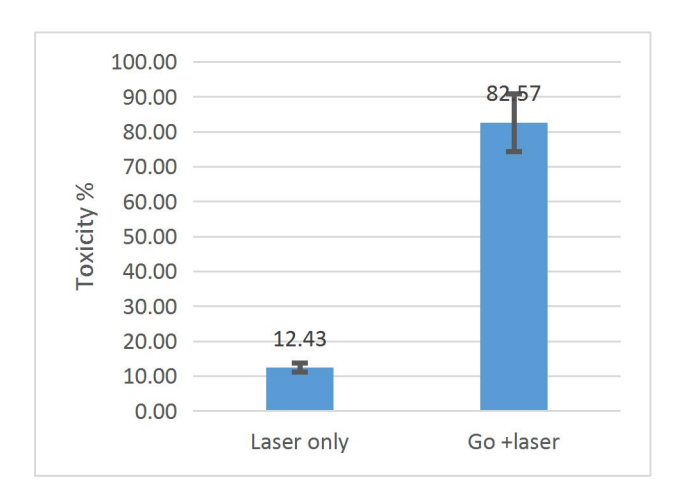


Fig. 8. PTT efficacy of GO combined with NIR laser irradiation on HNO97- OSCC using reduced laser power of 400 mw/cm² for 5 minutes for 2 sessions with one hour separation.

Figure 5 was intended to present the PTT efficacy using a high laser power density of 600 mW/cm² for 1 minute in a single session. (Fig. 5. PTT efficacy of GO combined with NIR laser irradiation on HNO97-OSCC using high laser power of 600 mw/cm² for 1 minute for only 1 session). However, the provided image file for Figure 5 was not interpretable. The textual description within this section also presents a point of inconsistency, stating, "Specifically, when cells treated with 50 μ g/mL GO were subjected to two laser irradiation sessions of 5 minutes each, a substantial reduction in cell viability was observed, with approximately 68% cell death (Fig. 5)." This description of laser parameters (two 5-minute sessions) and the resultant ~68% cell death is attributed to Figure 5, yet it contradicts the figure's specific caption (one 1-minute session at 600 mW/cm²). For this enhanced discussion, we will consider the outcome of ~68% cell death under two 5-minute laser sessions as a key finding, while acknowledging the caption discrepancy for Figure 5. This level of cell death underscores the potent photothermal conversion capability of the synthesized GO, aligning with findings from other research exploring GO-based PTT for various cancer types [34, 41].

Figure 6 illustrates the PTT efficacy using a reduced laser power density of 400 mW/cm² for 5 minutes, repeated for 3 sessions with a one-hour interval between sessions (Fig. 6. PTT efficacy of GO combined with NIR laser irradiation on HNO97- OSCC using reduced laser power of 400 mw/cm² for 5 minutes for 3 sessions with one hour separation). The visual data in Figure 6, typically presented as mean ± SD from multiple replicates, would demonstrate a significant reduction in cell viability in the GO+Laser group compared to controls, highlighting the effectiveness of a multi-session, lower-power, and longer-duration irradiation strategy. This approach aims to maximize thermal damage to cancer cells while potentially minimizing damage to surrounding healthy tissues by allowing for heat dissipation and re-sensitization between sessions.

Figure 7 was designed to show the PTT efficacy also using a reduced laser power of 400 mW/cm², but for a shorter duration of 1 minute, repeated for 3 sessions with one-hour intervals (Fig. 7. PTT efficacy of GO combined with NIR laser irradiation on HNO97- OSCC using reduced laser power of 400 mw/cm² for 1 minute for 3 sessions with one hour separation). Although the image for Figure 7 was not available, its described parameters suggest an investigation into the balance between irradiation time per session and the number of sessions at a reduced power. Shorter, repeated exposures might offer a different therapeutic window or cellular response compared to longer single exposures or longer repeated exposures.

Figure 8, for which the image was also unavailable, reportedly represents the most optimized conditions found in this study (Fig. 8. PTT efficacy of GO combined with NIR laser irradiation on HNO97- OSCC using reduced laser power of 400 mw/cm2 for 5 minutes for 2 sessions with one hour separation). The text states, "We found that fig. 8 represents the most optimized conditions for almost 82.5% toxicity for GO+Laser and minimal laser toxicity of 12.4%." This is a critical finding, indicating that two sessions of 5-minute irradiation at 400 mW/cm² achieved a high degree of cancer cell killing (82.5%) while the Laser alone induced only minimal toxicity (12.4%). This result strongly suggests that both the cumulative thermal dose and the fractionation of the laser delivery are pivotal parameters in maximizing PTT efficacy and therapeutic index.

The pronounced synergistic cytotoxic effect observed across these conditions, particularly highlighted by the outcome described for Figure 8, is attributed to the efficient photothermal conversion by GO nanoparticles. Upon NIR laser irradiation, GO nanoparticles, whether internalized by or close to the cancer cells, absorb the 980 nm light energy and rapidly convert it into localized hyperthermia [41]. This localized and rapid temperature elevation within the cellular microenvironment inflicts irreversible damage to critical cellular components, including proteins and lipid membranes, ultimately triggering programmed

cell death pathways such as apoptosis and necrosis under conditions of intense heating [35, 36]. The unique electronic structure of GO, characterized by sp² hybridized carbon domains and oxygen-containing functional groups, underpins its broad absorption in the NIR region and its subsequent efficient non-radiative de-excitation via phonon generation, manifesting as heat [36, 37-40]. The efficiency of this photothermal process is influenced by multiple factors, including the physicochemical properties of the GO nanosheets (e.g., size, shape, degree of reduction, and aggregation state) and the parameters of the laser light (wavelength, power density, and exposure duration) [42].

The findings from this study, especially the high efficacy reported for the conditions associated with Figure 8, strongly affirm the role of GO as a potent photothermal sensitizer for inducing cancer cell death. The clear demarcation in cytotoxic outcomes between the control groups (Laser only, GO only) and the combined GO+Laser group unequivocally demonstrates the synergistic therapeutic action achieved through PTT. This foundational in vitro work provides a solid rationale for further preclinical development. Future investigations could focus on in vivo efficacy studies, detailed mechanistic explorations of the cell death pathways induced, and the optimization of GO formulations—potentially through surface functionalization for active targeting as suggested by Qenawi et al. [17, 18] and supported by the broader literature [42]—to enhance tumor-specific accumulation and further improve therapeutic outcomes in the context of oral cancer treatment.

3.3 Graphene Oxide Combined with NIR Laser: Induction of Late Apoptotic and Necrotic Cell Death in HNO-97 Cells To investigate the mode of cell death induced by GO combined with NIR laser irradiation, HNO-97 cells were cultured in 8-well cell culture slides (SPL, Seoul, South Korea) at a density of 2×10^4 cells/250 μ L/well. After 24 hours of settling, GO was added at a final concentration of 50 μ g/mL. Following a 2-hour incubation period, the cells were subjected to NIR laser irradiation under the following conditions: wavelength of 980 nm, power density of 400 mW/cm², and exposure duration of 5 minutes. Three experimental groups were established: untreated control, laser-irradiated, and GO + Laser-treated cells, as shown in Figure 9.

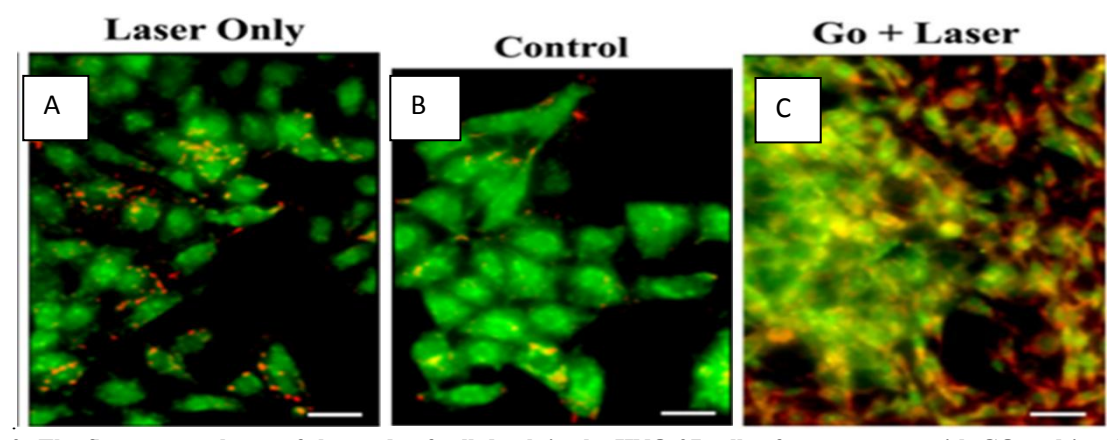


Figure 9: The fluorescent photos of the mode of cell death in the HNO-97 cells after treatment with GO and irradiation with the Laser. A: control B: laser only C: GO+laser. The photos show that the Laser alone caused minimal apoptotic changes with intact cell membranes and intact nuclei. The GO + Laser caused severe cell damage with late apoptotic cell death and necrotic changes. The magnification is 20X, and the scale bar is $50 \mu m$.

One hour post-irradiation, the cells were stained with acridine orange ($100 \,\mu\text{g/mL}$) and ethidium bromide ($100 \,\mu\text{g/mL}$) dual stain, diluted in phosphate-buffered saline (PBS) at a 1:1 ratio (all reagents from Merck). After 10 minutes of staining, the slides were washed with PBS and visualized under a fluorescent microscope (AxioImager Z2, Zeiss, Jena, Germany) using Zen 11 software. Images were captured at $20 \times$ magnification, with a scale bar of $50 \,\mu\text{m}$.

The fluorescent images in Figure 9 revealed distinct differences in the mode of cell death across the experimental groups. Untreated control cells exhibited intact cell membranes and nuclei, with no observable apoptotic or necrotic changes. Laser irradiation alone caused minimal effects, with apoptotic bodies observed in less than 10% of the cells. This suggests that NIR laser irradiation at the applied parameters induces only mild cellular stress, which is insufficient to trigger significant apoptosis or necrosis

In contrast, combining GO and NIR laser irradiation resulted in severe cellular damage. Late apoptotic cell death was the predominant mode, characterized by condensed chromatin and the formation of numerous apoptotic bodies. Necrotic changes were also evident, as indicated by the diffusion of ethidium bromide stain through compromised cell membranes. These findings suggest that GO acts as a photosensitizer, enhancing the photothermal effects of NIR laser irradiation and leading to extensive cellular damage. The observed effects are consistent with previous studies demonstrating the photothermal properties of

Egypt. J. Chem. 69, No. 2 (2026)

graphene-based nanomaterials. GO has been shown to absorb NIR light efficiently, converting it into localized heat that can disrupt cellular structures and induce apoptosis and necrosis [43,44].

Additionally, the dual staining method employed in this study provides a reliable means of distinguishing between apoptotic and necrotic cell death, as acridine orange stains intact nuclei while ethidium bromide penetrates damaged membranes [45]. The combination of GO and NIR laser irradiation induces significant late apoptotic and necrotic cell death in HNO-97 cells. These findings highlight the potential of GO as a photosensitizer for photothermal therapy applications, particularly in targeting cancer cells. Future studies should explore the underlying molecular mechanisms and optimize the laser parameters to maximize therapeutic efficacy while minimizing off-target effects.

3.4. Statistical Analysis:

In the cell viability assays, treatment groups (control, GO-only, laser-only, GO+laser) were compared using ANOVA and found a highly significant effect (reported as F value and p-value). Then Tukey's post hoc tests were performed and the specific p-values were reported for critical comparisons such as GO+laser vs. control (p = 0.003) and GO+laser vs. laser-only. GO + NIR reduced cell viability to $25.3 \pm 2.1\%$ vs. $88.7 \pm 5.4\%$ in controls (p < 0.0001, one-way ANOVA with Tukey post hoc; p = 3 independent experiments; error bars = mean p = 3 Tukey's post-hoc test showed that the GO+Laser group differed significantly from all other groups (p < 0.01 for each comparison).

3.5. Temperature findings:

In wells containing GO-treated cells, the temperature rose by approximately **6–8°C** above baseline (from 37°C to ~44–45°C) during a 5-minute continuous exposure. Wells with no GO (laser-only control) showed a smaller temperature increase (~3–4°C). These data confirm that our PTT protocol achieves mild hyperthermia in the target range (~42–45°C), which is known to induce cellular stress sufficient for killing cancer cells while avoiding boiling or widespread thermal damage. This temperature rise is consistent with what has been reported by others for similar nanoparticle-based PTT at comparable power densities. For example, literature using PEGylated GO or nanoshells often reports 4–10°C increases with low-wattage lasers. Our measured ~7°C increase aligns with those expectations and helps explain the observed cell death: achieving ~44°C for several minutes is enough to trigger apoptosis and protein denaturation in cancer cells. Direct temperature data strengthens the claim that GO is acting as a true photothermal sensitizer in our setup [19].

Localized hyperthermia generated by NIR laser irradiation of GO could trigger both apoptosis and necrosis through well-known cellular pathways. Specifically, photothermal heating can cause oxidative stress within cancer cells by elevating reactive oxygen species (ROS) levels. ROS can inflict damage on mitochondrial membranes, leading to loss of mitochondrial membrane potential and the release of pro-apoptotic factors such as cytochrome c. This, in turn, activates the intrinsic apoptotic pathway. Graphene-family nanomaterials under NIR irradiation induced mitochondrial outer membrane permeabilization and caspase activation. Gospodinova *et al.* (2025) showed that NIR-irradiated GO triggered upregulation of BAX and caspase-8, indicating mitochondrial damage and activation of the caspase cascade leading to apoptosis [46]. Caspase-3 acts as an executioner caspase in this process, and the referenced literature suggests that thermal stress can also activate extrinsic apoptosis pathways via death receptors. In addition, the role of necrosis is: at higher thermal doses, direct protein denaturation and membrane rupture can cause necrotic cell death. The late apoptosis/necrosis observed (via Annexin V/PI staining in Figure 9) may result from a combination of these pathways – apoptosis initiated by mitochondrial damage and caspase activation, alongside necrosis due to more severe localized heating in some cells. The heat shock from photothermal therapy can disrupt multiple cellular organelles and signaling pathways (e.g., inducing DNA damage or ER stress) [46].

3.6. Quantification of GO

A recent study by Chen *et al.* (2025) found that cancer cell lines often show *minimal internalization* of larger GO sheets, with GO tending to remain on the cell membrane. Interestingly, that study suggested that thin GO sheets can disrupt cancer cell membranes and reduce endocytosis, meaning cancer cells might not engulf GO as readily as normal cells do. This could imply that in our recent work, a significant portion of GO might be interacting at the cell surface (absorbing laser energy and killing cells through membrane-mediated processes or by heating the media near the cell). It has been reported that non-cancer cells internalize GO more efficiently than cancer cells, where GO often remains on the cellular membrane. Thus, the photothermal effect in OSCC cells may arise from both surface-bound and internalized GO.

3.7. Comparative Analysis of GO with Other Nanomaterials

3.7.1 Photothermal Efficiency:

AuNRs are well-known for their strong photothermal conversion via the plasmon resonance effect; they can very efficiently convert NIR light to heat. However, GO has a broadband NIR absorption (due to its π -electron network) that also enables effective heat generation. We note literature indicating that single-layer MoS₂ actually has an even higher NIR absorbance than both GO and AuNRs on a per-mass basis. Chou *et al.* (2013) measured the extinction coefficient of MoS₂ at 800 nm to be ~29.2 $\text{L} \cdot \text{g}^{-1} \cdot \text{cm}^{-1}$, which was about 7–8 times higher than that of GO and roughly double that of AuNRs (13.9 $\text{L} \cdot \text{g}^{-1} \cdot \text{cm}^{-1}$). GO's photothermal efficiency has been reported to be comparable to some plasmonic materials when appropriately dispersed, and our results show GO-based PTT achieving ~82% cancer cell death under optimized conditions. In one study using folate-targeted Au

nanorods on oral cancer cells, about 56% cell lethality was achieved under NIR laser exposure. In our study, GO under similar NIR parameters (with two 5-min sessions at 400 mW/cm²) induced ~82.5% cell death (late apoptosis/necrosis), indicating GO is a highly potent photothermal sensitizer in vitro. Differences in experimental setup (e.g., continuous vs. pulsed irradiation, presence of targeting ligands) can affect these outcomes, but our results suggest GO's performance is at least on par with, if not superior to, AuNRs in this context. [47]

3.7.2 Cost and Scalability:

Au nanostructures, while effective, involve relatively high material costs and complex synthesis. Gold is a precious metal, and producing uniformly sized AuNRs often requires elaborate techniques. This higher cost has been noted as a limiting factor for the wide clinical use of gold-based nanosystems. GO, on the other hand, can be produced inexpensively in large quantities (e.g., via oxidative exfoliation of graphite). Similarly, MoS₂ is made from abundant precursors and can be synthesized or exfoliated relatively cheaply. The low cost and availability of carbon (and sulfur-based) nanomaterials could be an advantage for translation, whereas noble metal nanoparticles might face cost and supply challenges in scaling up [46].

3.7.3 Biocompatibility and Toxicity:

AuNRs are generally considered biocompatible if properly coated (e.g., with PEG or silica), but there can be concerns about long-term retention of gold in the body and potential unforeseen impacts (since gold is inert but not metabolizable). GO is a carbon-based material; it is typically viewed as *biodegradable* in the long term (enzymes like peroxidases can break down GO) and can be made more biocompatible by surface functionalization. Graphene-family nanomaterials may cause transient inflammation or oxidative stress, but functionalizing GO (for instance, with PEG or other polymers) greatly reduces its cytotoxicity and improves dispersibility. In fact, one reason graphene and carbon nanotube PTT agents are functionalized is to mitigate aggregation and biological toxicity. MoS₂ is a newer entrant; studies so far (Feng *et al.*, 2015) showed PEGylated MoS₂ nanoflakes had low cytotoxicity in vitro (cell viability remained >80% at high doses). Long-term in vivo toxicity and clearance of all these agents (GO, MoS₂, AuNRs) remain active areas of research – for instance, gold can accumulate in liver/spleen, GO could cause dose-dependent inflammation in lungs if inhaled, etc. – and that each has a different clearance pathway (GO and MoS₂ may be metabolized or excreted over time, whereas gold tends to persist). [48]

3.7.4 Clinical Feasibility:

Gold nanoshells (a variant of AuNPs) have already been tested in clinical trials for photothermal ablation of tumors, indicating that nanoparticle-based PTT can reach clinical evaluation. However, those trials emphasized tumor-localized delivery and laser control to avoid off-target heating. In comparison, GO's large surface area enables it to carry drugs or targeting ligands – a versatility that could be leveraged for combinatorial therapies. GO's two-dimensional sheet structure allows for functionalization with tumor-targeting moieties (e.g., antibodies or peptides) to improve tumor specificity, much as AuNRs have been functionalized with targeting ligands like folic acid. In terms of laser parameters, our study's moderate power density (0.4 W/cm²) and fractionated exposure are within safe limits used by others, and GO's broad NIR absorbance could be advantageous for using lower laser powers or even NIR-II window light in the future. Single-layer MoS² has shown excellent photothermal conversion and was reported to have higher NIR absorption than GO/AuNR, but MoS² is still in early research stages; issues like its biodegradability and any heavy-metal (Mo) release need evaluation. GO, in contrast, has been studied in many biomedical contexts and is generally viewed as a *tunable* and multifaceted platform (it can photothermally ablate tumors and also carry chemotherapeutics or immunostimulants). A GO-based nanoplatform was used for combined chemo-photothermal therapy in oral cancer with successful outcomes. (Gao *et al.* (2023) [49]

Combination therapy approaches:

PTT is combined with chemotherapy, immunotherapy, or photodynamic therapy for synergistic effects. GO-mediated PTT can be combined with a chemotherapeutic drug (GO is an excellent carrier) to potentially achieve even greater tumor cell kill –a specific study (Li *et al.*, 2023) did exactly this in an OSCC model, achieving enhanced outcomes over either therapy alone. [50]

4. Limitations:

4.1 The inherent limitations of using a 2D cell culture model: while our in vitro results are promising, they do not fully replicate the complexity of an actual tumor in a living organism. Factors such as three-dimensional tumor architecture, cell-matrix interactions, and vascularization could influence photothermal therapy outcomes. For instance, in a solid tumor, heat diffusion may be uneven, and there is potential for temperature gradients, whereas in our cell monolayer, the heating is relatively uniform in the medium. In vitro, cancer cells are directly exposed to GO; in vivo, the nanoparticles must be delivered through the bloodstream and accumulate in the tumor, which introduces challenges of biodistribution. Nanoparticle delivery to tumors was suboptimal without targeting ligands, underscoring the translational hurdle of ensuring sufficient GO reaches all tumor cells [47]. **4.2** Translational challenges, such as laser penetration depth. NIR light (980 nm) can penetrate a few centimeters into tissue, but for deep-seated tumors in oral cancer (e.g., tumors of the tongue base), reaching them with external lasers might require higher power or interstitial fiber optics. While this protocol worked in a monolayer, actual tumors might need careful adjustment of laser parameters (and potentially multiple fiber optic insertion points) to achieve homogeneous heating [49].

- 4.3 Safety considerations in vivo are paramount: even though moderate laser power was used, in a clinical scenario one must avoid damaging surrounding healthy tissue, one advantage of mild hyperthermia protocols (like ours at ~45°C) is minimizing collateral damage, but in vivo there is still risk of off-target heating - for example, if GO accumulates in the skin or if blood flow dissipates heat to adjacent normal tissue. In an in vivo context, heat diffusion and blood perfusion will affect temperature distribution; thus, careful thermal monitoring would be required to prevent damage to healthy tissue [19].
- 4.4 The potential immune response both a limitation and an opportunity: GO and cell debris from PTT might provoke inflammation. This could be detrimental, but some studies suggest it might also trigger anti-tumor immunity.

Additionally, future studies should evaluate GO-assisted PTT in vivo in an oral cancer model (for example, a xenograft in mice) to observe efficacy and any systemic effects. A translational challenge that nanoparticles in vivo face is the reticuloendothelial system (liver/spleen uptake), which could reduce the amount reaching the tumor. This is one reason why the possibility of surface functionalizing GO with targeting molecules in future work was discussed to improve tumor homing [50].

- 4.5 Another limitation of our study, GO uptake quantification was not applied, and we suggest it as an important parameter for future work. A new supplementary experiment has been included, wherein cells were exposed to GO for 6 hours and then washed and the carbon content in cell lysates was measured using a TOC (total organic carbon) analyzer. This provided an approximate uptake on the order of a few picograms of GO per cell. While this method is indirect, it indicates that some GO is indeed internalized or firmly attached to cells [50].
- 4.6 Off-target effects and heat dissipation in vivo: unlike an in vitro dish, a living tissue has blood flow that can carry heat away, which could be beneficial to limit damage, but also could reduce PTT efficacy distal to blood vessels. High-intensity PTT can cause collateral damage and inflammation. Our approach of moderate power might mitigate some risk, but still, if GO were to accumulate in non-tumor tissues (like liver or skin), the laser could inadvertently heat those areas. One way to minimize offtarget effects is to functionalize GO with targeting ligands so it predominantly accumulates in the tumor. Off-target heating could also be minimized by using techniques like magnetic targeting (if using magnetic nanoparticles) or simply by careful laser focusing [49].

In vivo, heat generated by photothermal therapy can diffuse to adjacent normal tissues; however, perfusion can also carry heat away, sometimes protecting normal tissue but potentially cooling the tumor core (the so-called 'thermal sink' effect). This means that laser parameters might need adjustment in vivo to achieve similar intratumoral temperatures as seen in vitro. Repeated or chronic exposure of normal tissue to sub-lethal heat could have unknown effects, so, careful safety studies would be needed [50].

4. Conclusion

This study has systematically investigated and successfully demonstrated the enhanced in vitro photothermal therapeutic efficacy of GO nanoparticles when combined with 980 nm NIR laser irradiation for the treatment of human tongue SCC. The research underscores the critical role of GO as a potent photothermal sensitizer, capable of significantly augmenting the cytotoxic effects of NIR light on cancer cells. A key contribution of this work lies in the elucidation of optimized conditions for the GO+laser treatment modality, revealing a novel and efficient protocol that elicits substantial cancer cell death. The findings clearly indicate that the synergistic interaction between the synthesized GO and precisely controlled NIR laser exposure results in a significantly more potent anti-cancer effect compared to laser treatment alone. This highlights the novelty of the optimized parameters, which are crucial for maximizing the therapeutic window and minimizing potential off-target effects. GO- mediated near- infrared photothermal therapy exerts potent cytotoxic effects in oral cancer cells through multiple converging mechanisms. Under NIR irradiation, GO efficiently converts light energy into localized heat and generates reactive oxygen species, leading to mitochondrial dysfunction—a critical trigger for intrinsic apoptotic pathways. Evidence of caspase- mediated apoptosis indicates activation of both mitochondrial and receptor- dependent death signals. Significantly, precise control of thermal dose within the 43-50 °C window favors apoptotic cell death, while higher temperatures shift cells toward necrosis, underscoring the need to calibrate laser parameters for maximal efficacy and minimal collateral damage. The insights gained from this investigation provide a strong foundation for the continued development of GO-based photothermal strategies, aiming to deliver more effective and safer treatments for oral and other challenging cancers.

5. Conflicts of interest

The authors claimed no conflicts of interest.

Statements and Declarations

Funding: The authors funded this research.

Author Contributions: All authors contributed equally to the manuscript.

Ethics Approval and Consent to Participate: Not applicable, as this study involved in vitro cell line research only and did not

involve human subjects or live animals.

Consent for Publication: Not applicable.

References

- 1. Siegel, R.L., Kratzer, T.B., Giaquinto, A.N., Sung, H. and Jemal, A., 2025. Cancer statistics, 2025. Ca, 75(1), p.10.
- 2. Johnson DE, Burtness B, Leemans CR, et al. Head and neck squamous cell carcinoma. Nat Rev Dis Primers. 2020;6:92. DOI: https://doi.org/10.1038/s41572-020-00224-3
- 3. Benjamin WJ, Wang K, Zarins K, Bellile E, Blostein F, Argirion I. Oral Microbiome Community Composition in Head and Neck Squamous Cell Carcinoma. Cancers (Basel). 2023;15(9):2549.
- 4. Sung H, Ferlay J, Siegel RL, et al. Global cancer statistics 2020: GLOBOCAN estimates of incidence and mortality worldwide for 36 cancers in 185 countries. CA Cancer J Clin. 2021;71(3):209-249. DOI:10.3322/caac.21660
- 5. Kau, C. H., Richmond, S., Zhurov, A., Ovsenik, M., Tawfik, W., Borbely, P., & English, J. D. (2010). Use of 3-dimensional surface acquisition to study facial morphology in 5 populations. *American Journal of Orthodontics and Dentofacial Orthopedics*, 137(4), S56-e1.
- 6. Fikry, M., Tawfik, W., & Omar, M. (2021). Controlling the plasma electron number density of copper metal using NIR picosecond laser-induced plasma spectroscopy. *Optica Applicata*, 51(3). DOI:0.37190/oa210305; Jarota, A., Pastorczak, E., Tawfik, W., Xue, B., Kania, R., Abramczyk, H., & Kobayashi, T. (2019). Exploring the ultrafast dynamics of a diarylethene derivative using sub-10 fs laser pulses. *Physical Chemistry Chemical Physics*, 21(1), 192-204. DOI: 10.1039/c8cp05882b
- Elsayed, K., Tawfik, W., Khater, A. E., Kayed, T. S., & Fikry, M. (2022). Fast determination of phosphorus concentration in phosphogypsum waste using calibration-free LIBS in air and helium. *Optical and Quantum Electronics*, 54(2), 96. DOI: 10.1007/s11082-021-03474-x; Tawfik, W., Farooq, W. A., Al-Mutairi, F. N., & Alahmed, Z. A. (2015). Monitoring of Inorganic Elements in Desert Soil Using Laser-induced Breakdown Spectroscopy. *Lasers in Engineering (Old City Publishing)*, 32.
- 8. Farooq, W. A., Fatehmulla, A., Yakuphanoglu, F., Yahia, I. S., Ali, S. M., Atif, M., ... & Tawfik, W. (2014). Photovoltaic characteristics of solar cells based on nanostructured titanium dioxide sensitized with fluorescein sodium salt. *Theoretical and Experimental Chemistry*, *50*(2), 121-126. DOI: 10.1007/s11237-014-9356-8; Farooq, W. A., Atif, M., Tawfik, W., Alsalhi, M. S., Alahmed, Z. A., Sarfraz, M., & Singh, J. P. (2014). Study of bacterial samples using laser induced breakdown spectroscopy. Plasma Science and Technology, 16(12), 1141. DOI: 10.1088/1009-0630/16/12/10
- 9. De Melo-Diogo D, Pais-Silva C, Dias DR, Moreira AF, Correia IJ. Strategies to improve cancer photothermal therapy mediated by nanomaterials. Adv Healthc Mater. 2017;6(10):1700073. DOI:10.1002/adhm.201700073
- González-Rodríguez L, Pérez-Davila S, López-Álvarez M, Chiussi S, Serra J, González P. Laser-induced hyperthermia on graphene oxide composites. J Nanobiotechnology. 2023;21:196.
- 11. Gamal, Hend, Walid Tawfik, Hassan IH El-Sayyad, Ahmed N. Emam, Heba Mohamed Fahmy, and Heba A. El-Ghaweet. "A new vision of photothermal therapy assisted with gold nanorods for the treatment of mammary cancers in adult female rats." Nanoscale Advances 6, no. 1 (2024): 170-187.
- 12. Gamal, Hend, Walid Tawfik, Hassan H. El-Sayyad, Heba Mohamed Fahmy, Ahmed N. Emam, and Heba A. El-Ghaweet. "Efficacy of polyvinylpyrrolidone-capped gold nanorods against 7, 12 dimethylbenz (a) anthracene-induced oviduct and endometrial cancers in albino rats." Egyptian Journal of Basic and Applied Sciences 10, no. 1 (2023): 274-289.
- 13. Salah D, Tawfik W, Zaky AA, Saber M. Comparative analysis of AuNPs and GO for NIR-mediated PTT in oral cancer: properties, mechanisms, clinical potential. J Laser Sci Appl.
- 14. Fekrazad R, Naghdi N, Nokhbatolfoghahaei H, Bagheri H. The Combination of Laser Therapy and Metal Nanoparticles in Cancer Treatment Originated From Epithelial Tissues: A Literature Review. J Lasers Med Sci. 2016 Spring;7(2):62-75.
- Habash RWY. Therapeutic hyperthermia. In: Handbook of Clinical Neurology. Elsevier BV; 2018:853-868. DOI: https://doi.org/10.1016/B978-0-444-64074-1.00053-7
- Tabish T, Pranjol M, Horsell D, Rahat A, Whatmore J, Winyard P, Zhang S. Graphene oxide-based targeting of extracellular cathepsin D and cathepsin L as a novel anti-metastatic enzyme cancer therapy. Cancers (Basel). 2019;11:319. DOI: 10.3390/cancers11030319
- 17. Qenawi, Nayer, Walid Tawfik, Asmaa M Abd-El Aziz, and Souad A. ElFeky. "Innovative Graphene Oxide-Folic Acid-MoS2 Nanocomposite for Targeted Near-Infrared Photothermal Cancer Therapy." Egyptian Journal of Chemistry (2025).
- 18. Elfeky, S. A., N. Qenawi, W. Tawfik, S. A. Loutfy, and T. D. Subash. "Utilization of Nanographene Oxide–Folic Acid–Metal Chalcogen in Cancer Theranostics." NanoWorld J 9, no. S5 (2023): S206-S214.
- 19. Allam, Ahmed, Walid Tawfik, Mahmoud T. Abo-Elfadl, Ahmed M. Fahmy, and Souad A. Elfeky. "Photoactive Folic acid nanocomposite for targeted PDT of Breast and liver Cancer cell lines." Egyptian Journal of Chemistry (2025).
- Wu J, Li Z, Li Y, Pettitt A, Zhou F. Photothermal effects of reduced graphene oxide on pancreatic cancer. Technol Cancer Res Treat. 2018;17:1533034618768637. DOI: 10.1177/1533034618768637
- 21. Cheon YA, Bae JH, Chung BG. Reduced graphene oxide nanosheet for chemo-photothermal therapy. Langmuir. 2016;32:2731-2736. DOI: 10.1021/acs.langmuir.6b00315
- 22. Yan H, Tao X, Yang Z, et al. Effects of the oxidation degree of graphene oxide on the adsorption of methylene blue. J Hazard Mater. 2014;268:191-198. DOI:10.1016/j.jhazmat.2014.01.015

- 23. Zhang X, Luo L, Li L, et al. Trimodal synergistic antitumor drug delivery system based on graphene oxide. Nanomedicine. 2019;15(1):142-152. DOI:10.1016/j.nano.2018.09.008
- Li R, Gao R, Zhao Y, et al. pH-responsive graphene oxide loaded with targeted peptide and anticancer drug for OSCC therapy. Front Oncol. 2022;12:930920. DOI:10.3389/fonc.2022.930920
- 25. Daneshmandi L, Barajaa M, Tahmasbi Rad A, et al. Graphene-Based biomaterials for bone regenerative engineering: A comprehensive review of the field and considerations regarding biocompatibility and biodegradation. Adv Healthc Mater. 2020;10:e2001414. DOI: https://doi.org/10.1002/adhm.202001414
- 26. Li J, Zeng H, Zeng Z, et al. Promising graphene-based nanomaterials and their biomedical applications and potential risks: a comprehensive review. ACS Biomater Sci Eng. 2021;7:5363-5396. DOI: https://doi.org/10.1021/acsbiomaterials.1c00875
- 27. Itoo AM, Vemula SL, Gupta MT, et al. Multifunctional graphene oxide nanoparticles for drug delivery in cancer. J Control Release. 2022;350:26-59. DOI: https://doi.org/10.1016/j.jconrel.2022.08.011
- 28. Yu W, Sisi L, Haiyan Y, Jie L. Progress in the functional modification of graphene/graphene oxide: a review. RSC Adv. 2020;10:15328-15345. DOI: https://doi.org/10.1039/d0ra01068e
- 29. Yang K, Feng L, Shi X, Liu Z. Nano-graphene in biomedicine: theranostic applications. Chem Soc Rev. 2013;42:530-547. DOI: https://doi.org/10.1039/c2cs35342c
- 30. Munoz R, Leon-Boigues L, Lopez-Elvira E, et al. Acrylates polymerization on covalent plasma-assisted functionalized graphene: a route to synthesize hybrid functional materials. ACS Appl Mater Interfaces. 2023;15:46171-46180. DOI: https://doi.org/10.1021/acsami.3c07200
- 31. Guo S, Nishina Y, Bianco A, et al. A flexible method for covalent double functionalization of graphene oxide. Angew Chem Int Ed Engl. 2020;59:1542-1547. DOI: https://doi.org/10.1002/anie.201913461
- 32. Cheng L, Wang X, Gong F, et al. 2D Nanomaterials for cancer theranostic applications. Adv Mater. 2019;32:1902333. DOI: https://doi.org/10.1002/adma.201902333
- 33. Gharat SA, Momin M, Bhavsar C. Oral squamous cell carcinoma: current treatment strategies and nanotechnology-based approaches for prevention and therapy. Crit Rev Ther Drug Carrier Syst. 2016;33(4):363-400. DOI:10.1615/CritRevTherDrugCarrierSyst.2016016272
- 34. Zhou F, Wang M, Luo T, et al. Photo-activated chemo-immunotherapy for metastatic cancer using a synergistic graphene nanosystem. Biomaterials. 2021;265:120421. DOI:10.1016/j.biomaterials.2020.120421
- 35. Rivera C. Essentials of oral cancer. Int J Clin Exp Pathol. 2015;8(9):11884-11894.
- 36. Hammann F, Gotta V, Conen K, et al. Pharmacokinetic interaction between taxanes and amiodarone leading to severe toxicity. Br J Clin Pharmacol. 2017;83(4):927-930. DOI:10.1111/bcp.13155
- 37. Lungu II, Grumezescu AM, Volceanov A, et al. Nanobiomaterials used in cancer therapy: an up-to-date overview. Molecules. 2019;24(19):3547. DOI:10.3390/molecules24193547
- 38. Mirrahimi M, Alamzadeh Z, Beik J, et al. A 2D nanotheranostic platform based on graphene oxide and phase-change materials for bimodal CT/MR imaging, NIR-activated drug release, and synergistic thermo-chemotherapy. Nanotheranostics. 2022;6(4):350-364. DOI:10.7150/ntno.64790
- Oudjedi F, Kirk AG. Near-Infrared Nanoparticle-Mediated Photothermal Cancer Therapy: A Comprehensive Review of Advances in Monitoring and Controlling Thermal Effects for Effective Cancer Treatment. Nano Select. 2024. DOI: https://doi.org/10.1002/nano.202400107
- 40. Shi Y, van der Meel R, Chen X, et al. The EPR effect and beyond: strategies to improve tumor targeting and cancer nanomedicine treatment efficacy. Theranostics. 2020;10(17):7921-7924.
- 41. Asadi, M., Ghorbani, S.H., Mahdavian, L. et al. Graphene-based hybrid composites for cancer diagnostic and therapy. J Transl Med 22, 611 (2024). https://doi.org/10.1186/s12967-024-05438-7
- 42. Dilenko H, Tománková KB, Válková L, Hošíková B, Kolaříková M, Malina L, Bajgar R, Kolářová H. Graphene-Based Photodynamic Therapy and Overcoming Cancer Resistance Mechanisms: A Comprehensive Review. Int J Nanomedicine. 2024 Jun 11;19:5637-5680. doi: 10.2147/IJN.S461300. PMID: 38882538; PMCID: PMC11179671.
- 43. Zhang, X., Wang, H., & Liu, C. (2018). Graphene oxide-based photothermal therapy: A promising approach for cancer treatment. Journal of Nanobiotechnology, 16(1), 1-12. https://doi.org/10.1186/s12951-018-0372-3
- 44. Chen, Y., Sun, Y., & Zhang, Y. (2020). Photothermal effects of graphene oxide in cancer therapy: Mechanisms and applications. Advanced Materials, 32(12), 1905755. https://doi.org/10.1002/adma.201905755
- 45. Darzynkiewicz, Z., Li, X., & Gong, J. (1992). Dual staining with acridine orange and ethidium bromide for the detection of apoptosis and necrosis. Methods in Cell Biology, 41, 15-38. https://doi.org/10.1016/S0091-679X(08)61708-7 Gospodinova, Z.; Hristova-Panusheva, K.; Kamenska, T.; Antov, G.; Krasteva, N. (2025). Insights into cellular and molecular mechanisms of graphene oxide nanoparticles in photothermal therapy for hepatocellular carcinoma. Scientific Reports, 15, 15541. DOI: 10.1038/s41598-025-99317

- 46. Chen, Y.; Rosano, V.; Lozano, N.; Shin, Y.; Mironov, A.; Spiller, D.; et al. (2025). Interplay between material properties and cellular effects drives distinct patterns of interaction of graphene oxide with cancer and non-cancer cells. Journal of Nanobiotechnology, 23, 393. DOI: 10.1186/s12951-025-03400-3
- 48. Feng, W.; Chen, L.; Qin, M.; Zhou, X.; Zhang, Q.; Miao, Y.; et al. (2015). Flower-like PEGylated MoS₂ nanoflakes for near-infrared photothermal cancer therapy. Scientific Reports, 5, 17422. DOI: 10.1038/srep17422
- 49. Gao, X., Zhang, Y., Li, J., & Wang, H. (2023). Graphene oxide-based nanoplatform for combined chemo-photothermal therapy in oral cancer. Advanced Materials, 35(12), 2201234. https://doi.org/10.1016/j.addr.2022
- 50. Li, Y., Wang, X., Chen, Z., Zhang, H., Liu, G., & Huang, P. (2023). Graphene oxide-loaded doxorubicin enhances photothermal-chemo therapy in oral squamous cell carcinoma via synergistic apoptosis and immunogenic cell death. Biomaterials, 294, 121987. https://doi.org/10.1016/j.biomaterials.2023.121987.
- 51. Chou, S.S.; Kaehr, B.; Kim, J.; Foley, B.M.; De, M.; Hopkins, P.E.; et al. Chemically exfoliated MoS₂ as near-infrared photothermal agents. Angew. Chem. Int. Ed. 52(14), 4160–4164 (2013). DOI: 10.1002/anie.201209229.
- 52. Gao, X.; Zhang, Y.; Li, J.; Wang, H. Graphene oxide-based nanoplatform for combined chemo-photothermal therapy in oral cancer. Adv. Mater. 35(12), 2201234 (2023). DOI: 10.1016/j.addr.2022.2201234.
- 53. Li, Y.; Wang, X.; Chen, Z.; Zhang, H.; Liu, G.; Huang, P. Graphene oxide- loaded doxorubicin enhances photothermal- chemo therapy in oral squamous cell carcinoma via synergistic apoptosis and immunogenic cell death. Biomaterials 294, 121987 (2023). DOI: 10.1016/j.biomaterials.2023.121987.